

CURRENT-TRANSFORMER SATURATION RECONSTRUCTION USING A NORMALIZED LEAST MEAN SQUARES ADAPTIVE METHOD

AMIN SAREMI,¹ YOUNES MOHAMMADI,¹

DAVOOD KHODADAD,¹ BOŠTJAN POLAJŽER²

¹ Umeå University, Department of Applied Physics and Electronics, Umeå, Sweden
amin.saremi@umu.se, younes.mohammadi@umu.se, davood.khodadad@umu.se

² University of Maribor, Faculty of Electrical Engineering and Computer Science,
Maribor, Slovenia
bostjan.polajzer@um.si

This paper proposes a computationally light adaptive-filtering approach, normalized least mean squares (NLMS), to model the nonlinearity caused by the current transformer (CT) iron core saturation. A simplified CT model was used to generate a dataset considering four different nonlinear iron core magnetic characteristics. The preliminary results show satisfactory results in the cases where the CT iron core nonlinearity is within certain limits.

DOI
[https://doi.org/
10.18690/um.feri.4.2025.29](https://doi.org/10.18690/um.feri.4.2025.29)

ISBN
978-961-286-986-1

Keywords:

current transformer,
saturation,
reconstruction,
signal processing,
adaptive filter



University of Maribor Press

I Introduction

A well-known challenge in electrical power engineering is related to the saturation of the current transformer (CT) iron core. This phenomenon lowers measurement accuracy and may lead to the misoperation of protection relays. Several strategies have been suggested to mitigate the effects of CT iron core saturation, categorized into model-based, signal-processing and data-driven methods. A literature review on this topic can be found in [1–3].

This paper presents a solution based on the normalized least-mean-square (NLMS) adaptive method, commonly known as the Wiener filter. Adaptive filters, such as the NLMS method, have been utilized for decades for system identification tasks in control engineering, acoustics, and other signal-processing domains [4–5]. Despite the highly nonlinear nature of CT iron core saturation, we have explored how a computationally efficient linearized approach can still provide satisfactory predictions. In this approach, the model assumes that the system is semi-linear and adequately time-invariant within certain constraints. The objective is to identify the system by finding the finite impulse response of a linear model capable of closely approximating the input-output relationship.

II Method Description

A Dataset generation

Measured secondary currents I_s were obtained using a simplified CT model, neglecting windings resistance and leakage inductance. Thus, a first-order system with nonlinear feedback was used, with the nonlinearity capturing the magnetic characteristic of the iron core (flux versus mmf). Four different CT types were considered: CT1 with an over-sized iron core, CT2 with a standard-sized iron core, and CT3 and CT4 featuring an iron core with one or more air gaps.

Power system faults were simulated, where the magnitude of the pre-fault I_s was set as 1 A, whereas the steady-state magnitude of I_s during the fault was varied from 2 A to 15 A. Furthermore, different fault inception angles were used, including 0° , 45° , 90° . The time constant of the primary aperiodic component has also been varied in the range of 20 ms to 200 ms. In total, 798 cases were simulated, with a sampling

time of 0.5 ms used to generate the measured I_S . The desired I_S were generated similarly but using a CT model with linear magnetic characteristics.

Fig. 1 shows illustrative time responses for CT3, where steady-state of I_S was 10 A, with a fault inception angle of 90° and a 100 ms primary current time constant. The aperiodic component in the current causes an increase in the magnetic flux. The saturation effect is evident in the time responses of the nonlinear model, reflecting a distortion of the measured I_S .

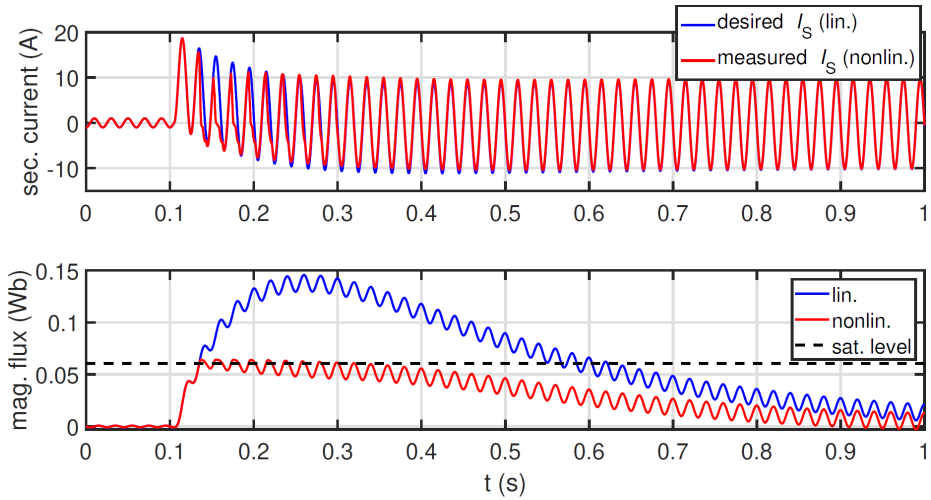


Figure 1: Time responses of linear and nonlinear models for CT3

B The NLMS adaptive algorithm

The dataset is divided into two parts. Half of the dataset (399 odd cases) is designed for training, and the remaining half (399 even cases) is reserved for the final evaluation of the method. The algorithm consists of two Wiener filters arranged in series. The first filter is 30 samples long (15 ms), whereas the second filter contains 40 samples (20 ms). For CT3 and CT4 datasets, however, both filters contain 40 samples. An initial impulse response $\hat{h}[n]$ is applied on the input signal $x[n]$, i.e., measured I_S , to generate an initial prediction $\hat{y}[n]$ according to (1), where $*$ denotes convolution.

$$\hat{y}[n] = x[n] * \hat{h}[n] \tag{1}$$

The error signal $e[n]$ is defined as the difference between the desired response $y[n]$, and the model's prediction $\hat{y}[n]$. The adaptation process occurs by estimating a new $\hat{h}[n]$ for each sample of $y[n]$ through a small adjustment by $\Delta\hat{h}[n]$ in each iteration, as expressed in (2) where $\mu[n]$ is 'step size'.

$$\begin{aligned} \hat{h}[n + 1] &= \hat{h}[n] + \Delta\hat{h}[n] \\ \Delta\hat{h}[n] &= \mu[n] (x[n] e[n]) \\ \mu[n] &= \frac{\alpha}{\beta + \sigma_{x[n]}^2}, \quad \sigma_{x[n]}^2 = x^T[n] x[n] \end{aligned} \quad (2)$$

Choosing an optimal step size is important for the system's accuracy and has been studied extensively [6]. In this study, we set $\beta = 0.01$, whereas α was assigned to 0.1 and 0.05 for the first and second filters, respectively.

The algorithm initially compares the input signal $x[n]$ with the entire training dataset to identify the closest case, yielding the maximum normalized correlation coefficient (NCC). Subsequently, it applies the filter coefficients obtained from the corresponding training case to the evaluation data. A representation of the described algorithm is shown in Fig. 3.

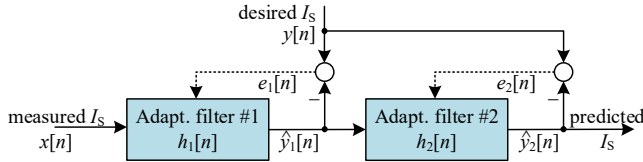


Figure 2: Blok diagram of the discussed adaptive algorithm

III Results

The predictions of the model $\hat{y}[n]$ were compared with the desired output $y[n]$. Mean Absolute Error (MAE), Root Mean Square Error (RMSE) and Total Vector Error (TVE) were calculated as follows:

- MAE = $\frac{1}{N} \sum_{i=1}^N (\text{abs}(\hat{y}[i] - y[i]))$, where N is the number of samples in the signal for 10 cycles after the fault inception;

- $RMSE[i] = \sqrt{\frac{1}{N} \sum_i^{i-N} (\hat{y}[i] - y[i])^2}$ computed for a one-cycle sliding window;
- $TVE[i] = \sqrt{(Re(\hat{Y}[i]) - Re(Y[i]))^2 + (Im(\hat{Y}[i]) - Im(Y[i]))^2}$ where $\hat{Y}[i]$ and $Y[i]$ are fundamental harmonic phasors computed for a one-cycle sliding window.

Furthermore, MAE, RMSE and TVE were calculated also for the measured I_s , i.e., by comparing the input $x[n]$ with the desired output $y[n]$. Metrics based on measured I_s are denoted as 'data', whereas metrics based on predicted I_s are denoted as 'model.' Fig. 4 shows an illustrative example for CT1, where steady-state of I_s was 9 A, the fault inception angle was 90° , and an 80 ms primary current time constant.

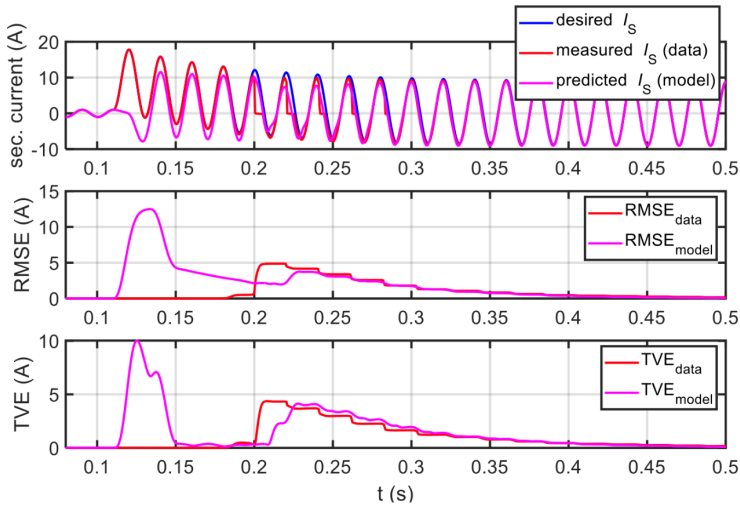


Figure 3: Results for CT1, where $MAE_{data} = 0.94$ A, $MAE_{model} = 3.13$ A

Fig. 5 shows MAE values for all evaluation cases related to CT1 as a function of the fault current magnitudes. The results show that the model is successful in the case of smaller fault current magnitudes (blue and red dots), generating more accurate results (smaller MAEs) than the data. However, the MAEs of the model are bigger than the MAEs of the data for higher fault current magnitudes (purple dots), which indicates the model's failure in those cases. Additionally, the time constant of the current's aperiodic component has a similar effect on MAE.

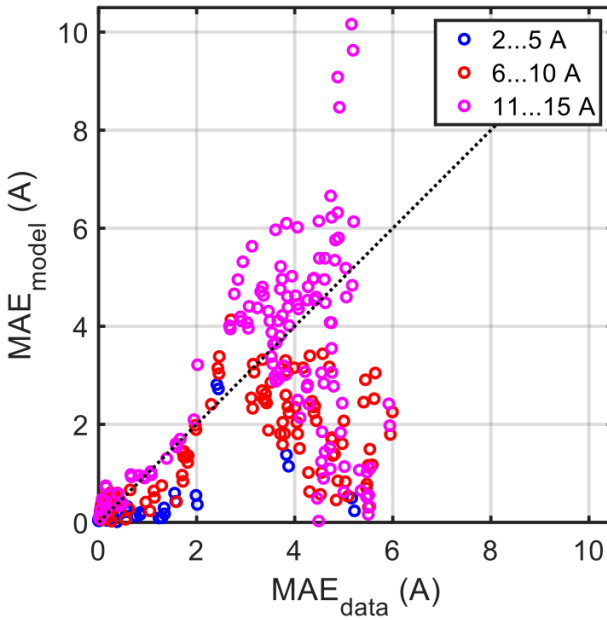


Figure 4. Comparison of MAE computed for the CT1 measurements (data) and predictions (model) for different values of the fault current magnitudes

IV Discussion and conclusions

Our objective was to explore the potential of adaptive filters, typically utilized for identifying semi-linear systems, in providing insights into iron core saturation in CTs. We deployed two Wiener filters to find the impulse response of the nearest linear system capable of producing comparable outputs. The code execution for all the 798 cases took less than 5 seconds on an Intel iCore 7 computer using MATLAB 2023b.

Preliminary results show that this approach could be effective for cases where CT nonlinearity falls within certain limits; however, it may fail for instances exceeding these limits. Although the discussed method is only partially successful, its computational simplicity and ease of implementation on real-time Digital Signal Processor (DSP) platforms warrant further investigation. Our next step involves quantifying the validity limits of our approach and applying it thoughtfully, ensuring successful prediction of the desired secondary currents.

References

- [1] L. Alderete, M.C. Tavares, F. Magrin, "Hardware implementation and real time performance evaluation of current transformer saturation detection and compensation algorithms", *Electr. Power Syst. Res.*, Vol. 196, 207288, 2021.
- [2] S. Key, S.-H. Kang, N.-H. Lee, S-Ry Nam, "Bayesian Deep Neural Network to Compensate for Current Transformer Saturation", *IEEE Access*, Vol. 9, pp. 154731-154739, 2021.
- [3] S. Yang, Y. Zhang, Z. Hao, Z. Lin, B. Zhang, "CT Saturation Detection and Compensation: A Hybrid Physical Model- and Data-Driven Method", *IEEE Trans. Power Del.*, Vol. 37, No. 5, pp. 3928-3938, 2022.
- [4] C. Paleologu, S. Ciochin, J. Benesty, S. L. Grant, "An overview on optimized NLMS algorithms for acoustic echo cancellation", *EURASIP J. Adv. Signal Process.*, 97, 2015.
- [5] A. Saremi, B. Ramkumar, G. Ghaffari, Z. Gu, "An acoustic echo canceller optimized for handsfree speech telecommunication in large vehicle cabins", *EURASIP J. Audio, Speech and Music Process.*, 39, 2023.
- [6] E. Hänsler, and G. Schmidt, *Acoustic echo and noise control: A practical approach*. Wiley, Hoboken, NJ, USA, 2004.

